Geol. Mag. **154** (*6*), *2017*, *pp. 1244–1256.* © *Cambridge University Press 2017*
doi:10.1017/S0016756817000206

Carbonate carbon isotope evolution of seawater across the Ediacaran–Cambrian transition: evidence from the Keping area, Tarim Basin, NW China

QINGJUN GUO*†‡, YINAN DENG§, JIAN HU¶ & LIYUAN WANG*||†

*Institute of Geographic Sciences and Natural Resources Research, Chinese Academy of Sciences, Beijing 100101, China
‡College of Resources and Environment, University of Chinese Academy of Sciences, Beijing 100049, China
§MLR Key Laboratory of Marine Mineral Resources, Guangzhou Marine Geological Survey, Guangzhou 510075, China
¶State Key Laboratory of Environmental Geochemistry, Institute of Geochemistry, Chinese Academy of Sciences, Guiyang Guizhou 550002, China
||College of Zijin Mining, Fuzhou University, Fuzhou 350116, China

(*Received* 2 November 2016; *accepted* 17 February 2017; *first published online* 10 April 2017)

Abstract – Sedimentary rocks from the Ediacaran–Cambrian boundary record important biological, climatic and geotectonic changes during this time. To date, only few geochemical investigations on the upper Ediacaran – upper Cambrian rocks in the Tarim Basin have been carried out. Here, we report high-resolution $\delta^{13}C_{carb}$ records from the Penglaiba, the Wushi phosphorite and the Dongergou sections from Ediacaran–Cambrian Series 3 in the Keping area of the Tarim Basin. The sections display several obvious $\delta^{13}C_{carb}$ shifts; $\delta^{13}C_{carb}$ values increased from 3 ‰ to 6.7 ‰ across the Qigebulage Formation. Moreover, a negative $\delta^{13}C_{carb}$ shift across the Ediacaran–Cambrian boundary is apparent; $\delta^{13}C_{carb}$ values decreased to a minimum of −9.8 ‰ in the Wushi phosphorite section (−7.7 ‰ in Dongergou section and −5.4 ‰ in Penglaiba section), followed by a positive carbonate carbon isotopic excursion across the Yuertusi Formation into the middle of the overlying Xiaoerbulak Formation. Furthermore, more or less invariable positive $\delta^{13}C_{carb}$ values characterize the middle and upper Xiaoerbulak Formation. The most negative $\delta^{13}C_{carb}$ value (−14.3 ‰) occurred near the base of the Shayilik Formation, which is the absolute minimum value among the studied sections of the Cambrian Series 2 to Cambrian Series 3 transition in the world. The $\delta^{13}C$ data from Keping, Tarim Basin are in good agreement with carbon isotope profiles recorded in South China, and these events may reflect the perturbation of the carbon cycle in the Tarim Basin during the Ediacaran–Cambrian and the Cambrian Series 2 – Cambrian Series 3 transitions.

Keywords: Ediacaran–Cambrian transition, Cambrian Series 2–3, carbon isotope, Tarim Basin, NW China

1. Introduction

Terminal Ediacaran and Cambrian successions worldwide record the consequences of profound geobiological changes in continental configuration, global climate, biological evolution, sea level and oxygen concentrations of the atmosphere at that time (e.g. Knoll, 1991; Zhu *et al.* 2003; Fike *et al.* 2006; Zhu, Strauss & Shields, 2007; Guo *et al.* 2010*a* , *b*, 2013; Maloof *et al.* 2010; Shields-Zhou & Och, 2011; Jiang *et al.* 2012; Schrag *et al.* 2013; Feng *et al.* 2014; Wang *et al.* 2015; Och *et al.* 2016). Numerous studies revealed the great chemostratigraphic potential of high-resolution carbon isotope records during the Precambrian–Cambrian transition (Brasier *et al.* 1994; Kaufman & Knoll, 1995; Brasier & Sukhov, 1998; Saltzman *et al.* 1998, 2000, 2004; Montañez *et al.* 2000), including many studies from the Yangtze Platform (Li *et al.* 1999, 2010, 2013; Shen & Schidlowski, 2000; Zhu *et al.* 2003, 2004; Guo *et al.* 2007, 2010*a*, *b*, 2013, 2014; G. Jiang *et al.* 2007, 2012; Zhou & Xiao, 2007; Zhu, Strauss & Shields, 2007; Sawaki *et al.* 2008; Zhao & Zheng, 2010). A relevant archive of sedimentary rocks from this time interval is well exposed in the Tarim Basin, China, including the preservation of different palaeoenvironmental settings. Similar sedimentary sequences between the Yangtze Platform and the Keping area of the Tarim Basin have been observed (Chen *et al.* 2004, 2010; Sun *et al.* 2004; Feng *et al.* 2006; He, Xu & Yuan, 2007; Yu *et al.* 2009).

The entire sedimentary succession comprises (in ascending stratigraphic order): limestone, dolostone, chert, black shale and phosphorite of the Ediacaran Qigebulage Formation and the lower Cambrian Yuertusi, Xiaoerbulak and Wusonger formations and the middle Cambrian Shayilik and Awatage formations. This sedimentary succession in the Tarim Basin is therefore well suited to uncover the interactions between atmosphere, hydrosphere, biosphere and lithosphere during this critical interval of Earth history. However, only a few geochemical studies (Chen *et al.* 2004, 2010; Sun *et al.* 2004; Feng *et al.* 2006; He, Xu & Yuan, 2007;

†Author for correspondence: guoqj@igsnrr.ac.cn

Figure 1. (Colour online) Geological map of the Tarim Basin (modified from Feng *et al.* 2006).

Yu *et al.* 2009) have been focused on the stratigraphy and the geological events in the Tarim Basin during the Ediacaran–Cambrian and Cambrian Series 2 – Cambrian Series 3 transitions. These are insufficient for comparison with the Yangtze Platform and other geological successions of the world, especially the division and the correlations of the stratigraphy between the Ediacaran–Cambrian and Cambrian Stage 4 – Stage 5 boundaries.

This study focuses on sedimentary rocks across the Ediacaran – Cambrian Series 3 transition in the Tarim Basin, NW China, considering the Penglaiba, the Dongergou and the Wushi phosphorite sections in western Xinjiang in particular (Fig. 1). One of the major aims was to investigate the link between high-resolution carbon isotope variations and the correlation with sections in other regions and referred to transgression. Moreover, the data can be used for supporting/refining the chemostratigraphic subdivision of the Ediacaran – Cambrian Series 3 boundary in China and elsewhere.

2. Geological setting and samples

The Tarim Basin is located in NW China, and contains sediments of the Ediacaran–Cambrian transition (Fig. 1). The Keping area in the northwestern part of the Tarim Basin provides good outcrop exposures from this time interval. During the Ediacaran–Cambrian transition, the Tarim Basin and the Yangtze platform were situated in a low-latitude position (Fig. 2) with similar depositional facies. This implies that the Tarim Basin is good for a regional stratigraphic division and correlation between both areas (Zhou 2001; Peng, 2009; Peng, Babcock & Cooper, 2012).

2.a. Penglaiba section

The Penglaiba section is located in Keping county, NW Xinjiang Uygur Autonomous Region. This section provides the most complete record including

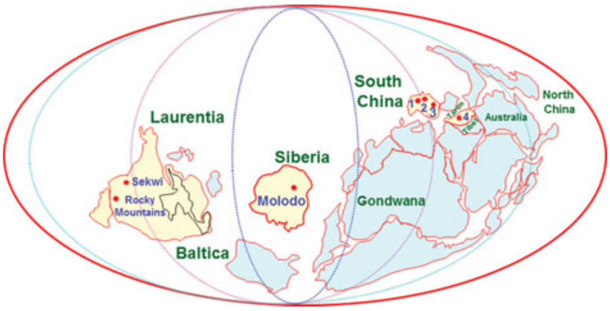

Figure 2. (Colour online) Palaeogeographic map during Ediacaran and Cambrian transition. (1) Lijiangtuo; (2) Wuliu-Zengjiayan; (3) Xiaotan; and (4) Penglaiba sections, China (modified from Scotese & McKerrow, 1990; McKerrow, Scotese & Brasier, 1992; Saltzman *et al.* 2000).

the Qigebulage, Yuertusi, Xiaoerbulak, Wusonger and Shayilik formations with no obvious depositional hiatus (Fig. 3). The Qigebulage Formation consists of carbonate and captures the transgressive Ediacaran–Cambrian boundary. The 20 m thick sequence of the Yuertusi Formation consists of black phosphatic siliceous rocks, phosphorite, black shale and dolostone and contains benthic small shelly fossils (Chen *et al.* 2004, 2010; Sun *et al.* 2004; Feng *et al.* 2006; He, Xu & Yuan, 2007; Yu *et al.* 2009). The overlying 114 m thick sequence of the Xiaoerbulak Formation consists of dolostone and intercalated limestone (Feng *et al.* 2006). Remains of trilobites, brachiopods, ostracods and small shelly fossils are common. The overlying Wusonger Formation, an 87 m thick sequence of dolostone and muddy dolostone (Feng *et al.* 2006), is time-equivalent to the uppermost Stage 3 and Stage 4, Cambrian Series 2 (Fig. 3a; Zhou, 2001; Peng, 2009). Trilobite species such as *Paokannia* sp. and *Redlichia* sp. from the *Paokannia zone* (Zhou, 2001) can be observed in the lower and middle part of the Wusonger Formation, which correlate to trilobite zones on the Yangtze Platform such as the *Ovatoryctocara granulate–Bathynotus holopygus* zone, the *Arthricocephalus jiangkouensis*,

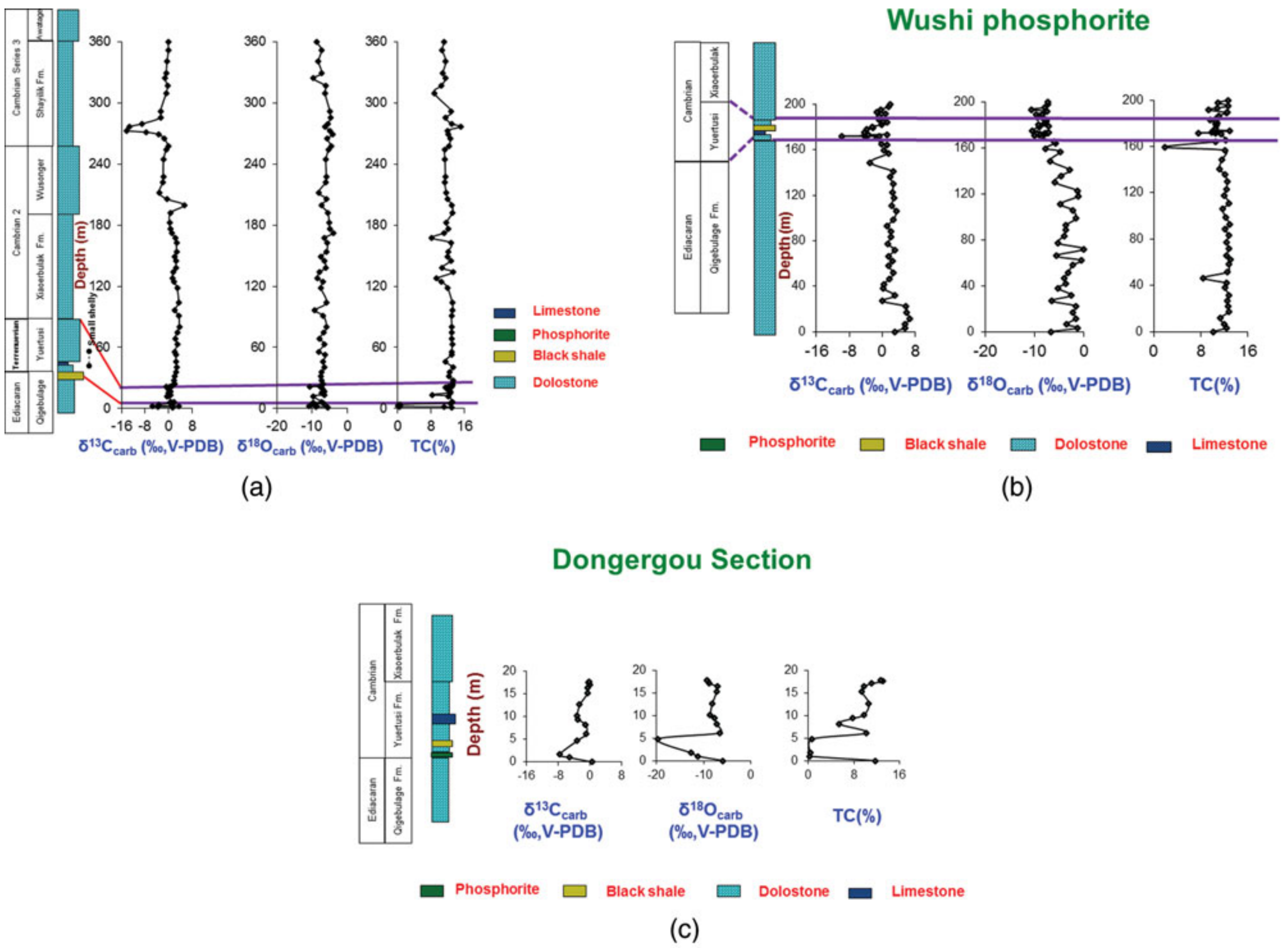

Figure 3. (Colour online) Comparison of temporal variations in $\delta^{13}C_{carb}$, $\delta^{18}O_{carb}$ and TC for the (a) Penglaiba, (b) Wushi phosphrite and (c) Dongergou sections.

Arthricocephalus chauveaui and *Arthricocephalites taijiangensis* zones (Zhou, 2001; Peng, 2009).

The 105 m thick sequence of the Shayilik Formation captures the transgressive Stage 4 – Stage 5 boundary (Cambrian Series 2 – Series 3; Fig. 3a; Zhou, 2001; Peng, 2009) and consists of dolostone, intercalated muddy dolostone and mudstone. The *Kunmingaspis–Chittidilla* trilobite zone (containing *Chittidilla nanjiangensis* Lu et Zhang, *Kunmingaspis kalpingensis* Zhang) of the Shayilik Formation in the Tarim Basin correlates with the *Oryctocephalus indicus* zone as well as the *Peronopsis taijiangensis* and *Peychagnostus gibbus* trilobite zones on the Yangtze Platform (Zhou 2001; Peng, 2009).

Seventy-two (72) samples were collected from the Penglaiba section for geochemical work in this study.

2.b. Wushi phosphorite section

The Wushi phosphorite section is located in Wushi county, Xinjiang Uygur Autonomous Region, and comprises sedimentary rocks of (in ascending stratigraphic order) the Qigebulage, Yuertusi and Xiaoerbulak formations (Fig. 3b). The 165 m thick Qigebulage Formation consists of dolostone and sandy dolostone, intercalated siltstone and sandstone, and there are abundant stromatolites, oncolites and micropalaeoflora in the formation. The overlying 24 m thick sequence of the Yuertusi Formation consists of phosphatic siliceous rocks, phosphorite, black shale and limestone. The boundary of the Ediacaran and the Cambrian is located between the Qigebulage and Yuertusi formations. The 11 m thick sequence of the Xiaoerbulak Formation consists of dolostone and siliceous dolostone. Fifty-nine (59) samples were collected from the Wushi phosphorite section for geochemical work in this study.

2.c. Dongergou section

The Dongergou section is located 60 km SW of Akesu city, Xinjiang Uygur Autonomous Region, and comprises sedimentary rocks of the Yuertusi Formation (Fig. 3c). This 16.5 m thick sequence consists of black phosphatic siliceous rocks, phosphorite, black shale and limestone with small shelly fossils (*Anabarites–Protohertzina*; Chen *et al.* 2004, 2010; Sun *et al.* 2004; Feng *et al.* 2006; He, Xu & Yuan, 2007; Yu *et al.* 2009). Fourteen (14) samples were collected from the Dongergou section for geochemical work in this study.

3. Analytical methods

Samples were chipped and pulverized (200 mesh). Total carbon (TC) abundances were measured at 1400 °C using a high-frequency infrared carbon and sulphur analyser at the Institute of Geographic Sciences and Natural Resources Research, Chinese Academy of Sciences. CO_2 for carbon and oxygen isotope analyses was liberated from whole-rock carbonates with phosphoric acid (McCrea, 1950; Wachter & Hayes, 1985) at 50 °C for 48 hours (dolostone) and 24 hours (limestone), respectively, and subsequent cryogenic distillation. All carbonate carbon and oxygen isotope analyses were carried out at the Institute of Geographic Sciences and Natural Resources Research, Chinese Academy of Sciences, using a ThermoFinnigan Delta Plus mass spectrometer. The analytical procedure was controlled by measuring the Beijing laboratory standard GBW 04406 for its $\delta^{18}O_{carb}$ ($\delta^{18}O_{carb\text{-}standard}$: −12.40 ‰; standard deviation: 0.20 ‰) and $\delta^{13}C_{carb}$ ($\delta^{13}C_{carb\text{-}standard}$: −10.85 ‰; standard deviation: 0.10 ‰) values. Results are reported in the standard delta notation as $\delta^{13}C$ and $\delta^{18}O$ v. VPDB. Standard deviations, as determined from replicate analyses, are generally better than 0.10 and 0.20 ‰ for carbon and oxygen isotopes, respectively.

In order to constrain carbonate diagenesis, samples were further studied for their elemental abundances of Mn, Sr, Fe, Ca and Mg (Veizer, 1983; Popp *et al.* 1986; Kaufman *et al.* 1993; Veizer *et al.* 1997, 1999). Samples were weighted and digested in 2N HCl and elemental concentrations were measured with atomic absorption spectroscopy at the Institute of Geographic Sciences and Natural Resources Research, Chinese Academy of Sciences. The precision is generally better than 5 %. Results were corrected for the amount of insoluble residue (soluble (%) = (total weight – weight insoluble residue)/total weight).

4. Results

4.a. Penglaiba section

A total of 72 samples from the following lithologies were analysed on TC abundance and carbon isotopic composition (Fig. 3a; Table 1): carbonates from Qigebulage Formation, phosphorite and carbonates at the Yuertusi Formation, dolostones of the Xiaoerbulak and Wusonger formations and carbonates of the Shayilik Formation. TC abundances vary over the range 8.5–13 wt % in the Qigebulage Formation, 0.4–13.2 wt % in the Yuertusi Formation, 9.4–13.3 wt % in the Xiaoerbulak Formation, 8.2–13.2 wt % in the Wusonger Formation and 8.7–15.1 wt % in the Shayilik Formation (Fig. 3a; Table 1).

$\delta^{13}C_{carb}$ values for sediments range from –2.9 ‰ to 6.7 ‰ in the Qigebulage Formation, from –5.4 ‰ to 3.5 ‰ in the Yuertusi Formation, from –0.7 ‰ to 3.7 ‰ in the Xiaoerbulak Formation, from –3.2 ‰ to 5.4 ‰ in the Wusonger Formation and from 0 ‰ to –14.3 ‰ in the Shayilik Formation (Fig. 3a; Table 1).

Elemental abundances of Mn and Sr are highly variable (Mn 0.003–0.078 %; Sr 0.003–0.039 %). Analytical results are given in Table 1.

4.b. Wushi phosphorite section

The carbonate carbon isotope result is based on 59 samples (Fig. 3b; Table 2), including carbonates from the Qigebulage Formation (165 m); across the Ediacaran–Cambrian transition; siliceous rocks, phosphorite and black shale at the base of Yuertusi Formation; and dolostones through the whole Yuertusi Formation.

Similar to the Penglaiba section, the base of the Yuertusi Formation in the Wushi phosphorite section consists of black phosphatic siliceous rocks, phosphorite and black shale (TC 0.3–1.8 wt %), whereas the lithology of the rest of the section is carbonate (TC 7.6–13.2 wt %).

$\delta^{13}C_{carb}$ values range between –2.9 ‰ and 6.7 ‰ in the Qigebulage Formation, and –9.8 ‰ and 1.1 ‰ in the Yuertusi Formation.

Elemental abundances of Mn and Sr are highly variable (Mn 0.003–0.141 wt %; Sr 0.002–0.041 wt %). Analytical results are given in Table 2.

4.c. Dongergou section

The Dongergou section comprises the Yuertusi Formation, which consists of black phosphatic siliceous rocks, phosphorite and black shale (TC 0.2–0.7 wt %), whereas the lithology of the rest of the formation is carbonate (TC 5.3–13.2 wt %).

Moreover, $\delta^{13}C_{carb}$ values vary from –7.7 ‰ to –0.1 ‰. Elemental abundances of Mn and Sr are highly variable (Mn 0.010–0.105 %; Sr 0.002–0.319 %). Analytical results are given in Table 3.

5. Carbonate diagenesis

Primary depositional trends from carbonate reflect seawater chemistry; however, carbonate diagenesis can change the elemental abundances and isotopic compositions of carbon and oxygen significantly (e.g. Veizer, 1983; Marshall, 1992). Most frequently, an increase in the abundance of Mn, a decrease in the Sr concentration and a decrease in $\delta^{13}C_{carb}$ and $\delta^{18}O$ (e.g. Veizer, 1983; Marshall, 1992) reflect progressing diagenesis.

Usually, a Mn/Sr ratio <5 (even better is Mn/Sr ratio <2) and $\delta^{18}O$ values more positive than –10 ‰ (even better is positive than –5 ‰) (Kaufman & Knoll, 1995) suggest that a carbonate has been retained near primary carbon isotope values and has archived past seawater chemistry.

No correlation can be observed between the carbonate carbon and oxygen isotopic compositions of the sedimentary rocks from the Yuertusi, Wusonger and Shayilik formations of the Penglaiba section, whereas a correlation is apparent between the

Table 1. Analytical results for sediments from the Penglaiba section, Tarim Basin, NW China.

Samples	Unit	Lithology	Depth (m)	TC (%)	$\delta^{13}C_{carb}$ (‰, VPDB)	$\delta^{18}O_{carb}$ (‰, VPDB)	Ca (wt%)	Fe (wt%)	Mg (wt%)	Mn (%)	Sr (%)	Mn/ Sr	Mg/ Ca
Plb 1	Qigebulage Fm.	Dolostone	1.2	13.03	1.3	–5.6	18.10	0.28	12.01	0.031	0.005	6.52	0.66
Plb 5		Dolostone	1.6	11.16	1.5	–5.7	19.97	0.25	10.97	0.027	0.009	2.87	0.55
Plb 6	Yuertushi Fm.	Siliceous rocks	1.8	0.41	–3.6	–8.9	2.25	1.15	0.11	0.074	0.007	10.39	0.05
Plb 8		Siliceous rocks	2.15	0.15	3.5	–10.9							
Plb 10		Mudstone	2.6	0.20	–5.4	–8.7	1.45	0.27	0.11				
Plb 12		Siliceous rocks	2.9	0.17									
Plb 13		Siliceous mudstone	4	0.61	–3.4	–10.2	1.99	1.60	0.05	0.077	0.009	8.57	0.03
Plb 15		Siliceous dolostone	5.4	12.65	1.7	–6.8							
Plb 16		Muddy dolostone	5.75	13.04	0.4	–9.7	14.45	0.17	12.20	0.025	0.004	6.27	0.84
Plb 17		Muddy dolostone	6.15	13.21	2.0	–7.2	20.86	0.22	11.54	0.014	0.021	0.68	0.55
Plb 18		Muddy dolostone	12.15	12.09	–0.6	–9.7	22.19	0.37	11.84	0.055	0.007	7.71	0.53
Plb 22		Muddy dolostone	13.5	8.23	0.7	–6.6	12.26	0.60	6.55	0.036	0.008	4.66	0.53
Plb 25		Dolostone	15.5	12.65	0.0	–7.2	22.14	0.44	13.17	0.077	0.004	17.18	0.59
Plb 27		Dolostone	17	12.68	0.6	–6.5	21.61	0.49	13.15	0.078	0.004	19.21	0.61
Plb 29		Dolostone	19	12.03	0.0	–6.9	16.10	0.48	9.59	0.063	0.004	14.96	0.60
Plb 31		Dolostone	20.7	11.42	0.6	–7.3	20.63	0.12	12.45	0.018	0.007	2.56	0.60
Plb 33	Yuertushi Fm.	Dolostone	21.6	12.98	0.4	–7.6	17.95	0.14	11.53	0.042	0.004	9.78	0.64
Plb 34	Xiaoerbulak Fm.	Dolostone	21.7	12.13	–0.7	–10.6	21.16	0.28	13.00	0.018	0.006	2.94	0.61
Plb 36		Dolostone	23	13.16	1.3	–7.3							
Plb 37		Dolostone	24	13.15	2.1	–7.0	14.86	0.07	12.40	0.017	0.003	5.82	0.83
Plb 38		Dolostone	27.5	13.29	1.9	–7.3	17.78	0.04	9.34	0.016	0.005	3.23	0.53
Plb 41		Dolostone	31.6	12.34	2.2	–7.6	19.19	0.07	12.81	0.015	0.005	3.03	0.67
Plb 43		Dolostone	36	12.43	2.6	–7.3	20.11	0.07	12.74	0.013	0.005	2.58	0.63
Plb 45		Dolostone	40.5	13.26	2.8	–6.5	21.13	0.06	12.88	0.011	0.007	1.53	0.61
Plb 47		Dolostone	46.3	11.44	2.7	–6.8	21.50	0.08	12.97	0.012	0.007	1.80	0.60
Plb 48		Dolostone	52.7	12.92	2.5	–6.2	21.47	0.04	13.41	0.012	0.006	1.90	0.62
Plb 49		Dolostone	55.6	13.00	2.1	–8.1							
Plb 50		Dolostone	63.3	13.08	3.0	–6.6	21.11	0.04	13.13	0.010	0.006	1.83	0.62
Plb 52		Dolostone	68.7	12.94	2.3	–7.8	20.68	0.04	12.80	0.010	0.005	2.02	0.62
Plb 53		Dolostone	74.5	12.96	2.9	–6.8							
Plb 54		Dolostone	80	13.02	3.7	–5.9	20.87	0.05	12.80	0.010	0.009	1.12	0.61
Plb 56		Dolostone	91.2	12.93	3.6	–6.8	20.33	0.04	12.59	0.011	0.006	1.86	0.62
Plb 57		Dolostone	96.4	13.24	2.1	–9.2							
Plb 58		Dolostone	104	13.11	3.5	–5.9	21.16	0.04	13.34	0.011	0.004	2.57	0.63
Plb 60		Dolostone	118.6	11.96	2.9	–7.6	20.12	0.04	12.73	0.008	0.003	2.41	0.63
Plb 115		Dolostone	124.7	10.48	1.9	–6.9							
Plb 116		Dolostone	127.7	9.36	1.4	–8.5	18.62	0.04	11.82	0.008	0.003	2.86	0.63
Plb 62		Dolostone	133.8	13.29	1.6	–7.9							
Plb 64		Dolostone	138.1	10.68	2.5	–6.2	19.01	0.04	11.92	0.007	0.003	2.41	0.63
Plb 68		Dolostone	144.9	12.77	2.6	–6.5							
Plb 118		Dolostone	148.8	11.98	2.2	–7.6	20.41	0.04	12.90	0.008	0.003	2.52	0.63
Plb 70		Dolostone	154.1	12.15	2.7	–6.0							
Plb 71	Xiaoerbulak Fm.	Dolostone	162.4	12.84	2.7	–5.7	21.03	0.06	13.17	0.009	0.005	1.78	0.63
Plb 75	Wusonger Fm.	Dolostone	167.4	8.19	2.2	–6.5							
Plb 74		Dolostone	172.2	11.13	1.2	–3.9	18.31	0.18	10.84	0.012	0.007	1.73	0.59
Plb 76		Dolostone	176.3	12.14	0.7	–5.0							
Plb 78		Dolostone	182.2	11.69	0.4	–5.2	18.58	0.20	11.27	0.011	0.006	1.67	0.61
Plb 80		Dolostone	192.2	13.17	0.8	–5.6	20.86	0.18	12.47	0.014	0.007	2.11	0.60
Plb 82		Dolostone	199.7	13.07	5.4	–7.3							
Plb 83		Dolostone	205.6	12.02	–0.5	–5.8	21.36	0.46	12.44	0.019	0.006	3.22	0.58
Plb 85		Dolostone	212	11.66	–3.2	–8.2	20.46	0.70	11.90	0.028	0.009	3.00	0.58
Plb 86		Dolostone	222.3	11.25	–1.8	–6.1	13.74	0.81	8.71	0.017	0.006	2.72	0.63
Plb 87		Dolostone	227.4	11.45	–1.8	–6.0							
Plb 88		Dolostone	244.4	11.35	–1.6	–6.1	18.84	0.90	11.32	0.017	0.008	2.19	0.60
Plb 89	Wusonger Fm.	Dolostone	254.3	11.26	–0.7	–5.3							
Plb 92	Shayilik Fm.	Dolostone	257.4	12.35	0.0	–4.5	21.84	0.34	13.00	0.010	0.009	1.14	0.60
Plb 93		Dolostone	264.7	12.62	–1.4	–5.7							
Plb 94		Dolostone	269	12.19	–3.4	–4.1	18.38	1.27	10.73	0.010	0.008	1.32	0.58
Plb96		Dolostone	271.2	11.35	–7.6	–4.5							
Plb 97		Dolostone	272.8	11.92	–14.3	–5.0	19.35	0.75	11.28	0.009	0.009	1.00	0.58
Plb 95		Dolostone	276.6	15.12	–13.4	–6.4	22.63	0.23	14.32	0.013	0.012	1.08	0.63
Plb 98		Dolostone	279.4	12.92	–9.0	–5.5	19.29	0.28	10.97	0.017	0.010	1.62	0.57
Plb 99		Dolostone	285.4	11.56	–2.7	–4.8							
Plb 100		Dolostone	291.8	12.90	–2.8	–5.0	24.69	0.34	13.31	0.010	0.009	1.17	0.54
Plb 101		Dolostone	309.6	8.74	–0.8	–6.4	16.24	0.79	9.03	0.030	0.011	2.83	0.56
Plb 102		Dolostone	316.6	10.49	–0.4	–6.2							
Plb 104		Dolostone	324	11.48	–1.2	–9.7	36.26	0.08	0.99	0.004	0.020	0.18	0.03
Plb 106		Dolostone	329.1	10.85	–0.8	–7.3							
Plb 107		Dolostone	340.7	11.56	–0.4	–8.2	30.35	0.05	1.30	0.003	0.019	0.17	0.04
Plb 109		Dolostone	351.9	10.73	0.0	–7.4	30.81	0.07	4.86	0.005	0.014	0.33	0.16
Plb 110	Shayilik Fm.	Dolostone	359.5	11.23	–0.1	–8.7	26.86	0.03	0.22	0.004	0.038	0.10	0.01
Plb 112	Awatage Fm.	Dolostone	360.7	11.32									

Table 2. Analytical results for sediments from the Wushi phosphorite section, Tarim Basin, NW China.

Samples	Unit	Lithology	Depth (m)	TC (%)	$\delta^{13}C_{carb}$ (‰, VPDB)	$\delta^{18}O_{carb}$ (‰, VPDB)	Ca (wt%)	Fe (wt%)	Mg (wt%)	Mn (%)	Sr (%)	Mn/Sr	Mg/Ca
WS 59	Qigebulage Fm.	Dolostone	0	10.1	3.0	−6.7	18.84	1.38	10.58	0.048	0.006	7.437	0.562
WS 62		Dolostone	3.3	12.33	5.5	−1.3							
WS 63		Muddy dolostone	6.3	12.03	5.5	−3.5							
WS 65		Mudstone	11.5	11.28	6.7	−1.7	20.21	0.41	11.38	0.018	0.008	2.263	0.563
WS 67		Dolostone	17	12.72	5.9	−2.3							
WS 69		Dolostone	22.2	12.64	5.7	−1.6	10.70	0.24	8.09	0.003	0.003	1.024	0.756
WS 71		Dolostone	26.9	12.49	0.0	−6.5							
WS 73		Dolostone	31.6	12.73	3.1	−2.6	21.76	0.25	12.89	0.008	0.007	1.065	0.592
WS 76		Dolostone	37.8	12.13	0.2	−5.3							
WS 78		Dolostone	41.8	12.41	0.3	−3.7	20.69	0.21	11.82	0.005	0.006	0.859	0.571
WS 80		Dolostone	46.4	8.451	1.8	−4.0							
WS 82		Dolostone	51.5	12.53	2.7	−3.1	21.72	0.19	13.04	0.010	0.003	3.096	0.600
WS 84		Dolostone	58	12.77	1.5	−2.3							
WS 86		Dolostone	62	13.01	2.6	−0.5	21.87	0.15	12.44	0.004	0.009	0.410	0.569
WS 88		Dolostone	66	12.33	1.6	−5.6							
WS 3		Dolostone	71.9	12.83	3.0	−0.1	21.99	0.14	12.97	0.003	0.003	1.022	0.590
WS 4		Dolostone	76.9	12.32	1.4	−5.2							
WS 5–1		Dolostone	83.3	12.72	2.1	−4.0	22.69	0.08	13.37	0.006	0.004	1.638	0.589
WS 7		Dolostone	88.4	12.14	2.2	−3.6							
WS 8		Dolostone	92.7	12.96	1.2	−3.7	23.25	0.13	14.02	0.006	0.005	1.291	0.603
WS 11		Dolostone	98.5	12.24	2.8	−1.6							
WS 12		Dolostone	105.8	11.74	3.3	−2.3	21.31	0.17	12.31	0.007	0.003	2.600	0.578
WS 13–1		Dolostone	111.1	12.8	2.2	−4.8							
WS 15		Dolostone	117.7	12.01	2.9	−1.2	23.09	0.10	13.97	0.006	0.002	2.866	0.605
WS 16		Dolostone	122.7	12.35	2.5	−1.3							
WS 18		Dolostone	129.9	12.45	2.6	−5.9	22.78	0.15	13.54	0.012	0.002	4.953	0.595
WS 20		Dolostone	135.8	12.09	1.8	−4.6							
WS 21		Dolostone	140.7	11.13	2.6	−2.9	21.94	0.25	12.84	0.010	0.020	0.505	0.585
WS 22–1		Limestone	148.7	11.59	−2.9	−6.8	36.63	0.20	0.30	0.022	0.030	0.729	0.008
WS 24		Dolostone	156.6	12.17	1.5	−4.8	18.98	0.16	10.99	0.022	0.004	5.994	0.579
WS 24–1		Breccia	159.4	1.85	0.4	−7.9							
WS 25		Dolostone	164	10.45	1.1	−5.7							
WS 25–1	Qigebulage Fm.	Dolostone	165	12.23	−0.2	−6.0	18.23	0.36	10.77	0.037	0.005	7.545	0.591
WS 27	Yuertusi Fm.	Muddy dolostone	170.6	11.4	−1.3	−10.0	21.83	0.31	11.05	0.053	0.019	2.718	0.506
WS 28		Sandy dolostone	171.6	10.53	−0.8	−9.0							
WS 29		Muddy dolostone	171.7	7.615	−9.8	−8.1							
WS 30		Muddy dolostone	172.05	10.39	−3.7	−8.1							
WS 31		Muddy dolostone	172.35	9.847	−4.3	−8.9	13.08	0.10	7.90	0.016	0.002	6.693	0.604
WS 32		Muddy limestone	172.65	10.02	−4.3	−9.5	35.19	1.04	0.41	0.033	0.023	1.414	0.012
WS 33		Muddy dolostone	172.85	10.43	−3.7	−7.8							
WS 34–1		Muddy dolostone	172.86	10.45	−3.3	−7.3							
WS 34–4		Muddy dolostone	173.41	12.91	1.1	−7.2	22.41	0.19	13.35	0.013	0.004	2.999	0.596
WS 35		Muddy dolostone	174.15	10.25									
WS 36		Muddy limestone	175.15	10.5	−4.3	−10.5	37.89	0.77	0.53	0.141	0.026	5.397	0.014
WS 38		Muddy dolostone	178.25	10.64	−3.8	−9.1							
WS 39		Muddy limestone	179.25	10.51	−2.3	−7.2							
WS 40		Muddy limestone	180.25	10.78	−2.5	−9.2	24.79	0.70	0.43	0.045	0.021	2.117	0.017
WS 41		Muddy dolostone	181.75	10.46	−0.2	−8.0							
WS 42		Muddy limestone	182.65	9.609	−0.1	−7.6	37.01	0.56	0.49	0.052	0.028	1.864	0.013
WS 44		Muddy limestone	184.15	10.61	1.1	−7.6	36.38	0.38	0.61	0.018	0.041	0.437	0.017
WS 45		Muddy dolostone	184.75	10.98	0.1	−8.1							
WS 47		Muddy dolostone	186.45	11.07	−0.8	−9.4	17.70	1.55	7.99	0.093	0.011	8.765	0.452
WS 50	Yuertusi Fm.	Muddy dolostone	189.05	12.41	−0.7	−8.4	24.35	0.34	12.52	0.060	0.006	10.295	0.514
WS 51	Xiaoerbulak Fm.	Dolostone	189.3	12.44	−0.7	−9.6							
WS 54		Dolostone	191.7	9.333	0.9	−7.5	16.53	0.06	9.12	0.011	0.004	2.485	0.552
WS 55		Dolostone	193.2	10.8	−1.3	−10.7							
WS 56		Dolostone	195.1	12.7	−0.3	−7.9	11.79	0.13	6.94	0.036	0.002	17.400	0.589
WS 57		Dolostone	197.7	10.96	1.6	−7.4							
WS 58	Xiaoerbulak Fm.	Dolostone	200	12.66	1.9	−7.2	21.80	0.11	13.06	0.013	0.005	2.611	0.599

carbonate carbon and oxygen isotopic compositions in the Xiaoerbulak Formation of the Penglaiba section (Fig. 4a). Moreover, a correlation is visible between the carbonate carbon and oxygen isotopic compositions of the sedimentary rocks from the Xiaoerbulak and Qigebulage formations of the Wushi phosphorite section (Fig. 4b), but no correlation could be observed between the carbonate carbon and oxygen isotopic compositions of the sedimentary rocks from the Yuertusi Formation of the Wushi phosphorite section.

In contrast, an obvious correlation between the carbonate carbon and oxygen isotopic compositions of the carbonate from the Yuertusi Formation of the Dongergou section could be detected (Fig. 4c). Positive correlations between oxygen and carbon isotopes are probably a result of diagenesis or late alteration.

Table 3. Analytical results for sediments from the Dongergou section, Tarim Basin, NW China.

Samples	Unit	Lithology	Depth (m)	TC (%)	$\delta^{13}C_{carb}$ (‰, VPDB)	$\delta^{18}O_{carb}$ (‰, VPDB)	Ca (wt%)	Fe (wt%)	Mg (wt%)	Mn (%)	Sr (%)	Mn/ Sr	Mg/ Ca
DRG 0	Qigebulage Fm.	Sandy dolostone	0	11.72	0.6	–6.0	17.89	0.42	10.00	0.027	0.004	6.1	0.56
DRG 1	Yuertusi Fm.	Phosphorite	1	0.24	–5.1	–11.2	18.76	1.17	0.21	0.010	0.319	0.0	0.01
DRG 3		Phosphorite	1.7	0.30	–7.7	–12.7	9.36	0.68	0.12	0.013	0.045	0.3	0.01
DRG 9		Mudstone	4.76	0.64	–3.1	–19.7	0.56	1.22	0.17	0.105	0.021	5.0	0.31
DRG 12		Dolostone	6.16	10.25	–1.0	–6.6	11.50	1.09	5.07	0.036	0.053	0.7	0.44
DRG 14		Dolostone	8.16	5.37	–1.1	–7.3	9.67	1.59	5.22	0.039	0.010	3.9	0.54
DRG 18		Limestone	9.36	7.85	–3.0	–7.7	12.26	0.31	0.40	0.011	0.009	1.3	0.03
DRG 19		Limestone	10.2	9.78	–3.3	–8.6	26.04	0.36	0.71	0.035	0.022	1.6	0.03
DRG 22		Limestone	12.6	10.65	–2.6	–8.2	25.56	0.26	0.42	0.020	0.022	0.9	0.02
DRG 24		Dolostone	15.2	9.37	–0.5	–7.3	15.09	1.28	9.10	0.045	0.009	4.8	0.60
DRG 27		Dolostone	16.4	9.80	–0.5	–7.1	19.94	1.07	12.48	0.062	0.009	6.9	0.63
DRG 29		Dolostone	17.1	11.06	–0.1	–8.9	6.56	0.47	5.85	0.027	0.002	15.5	0.89
DRG 31	Yuertusi Fm.	Dolostone	17.5	13.15	–0.3	–9.2	15.65	0.23	11.48	0.033	0.004	8.9	0.73
DRG 32	Xiaoerbulak Fm.	Dolostone	17.7	12.65	–0.2	–9.3	20.61	0.30	12.73	0.036	0.006	5.8	0.62

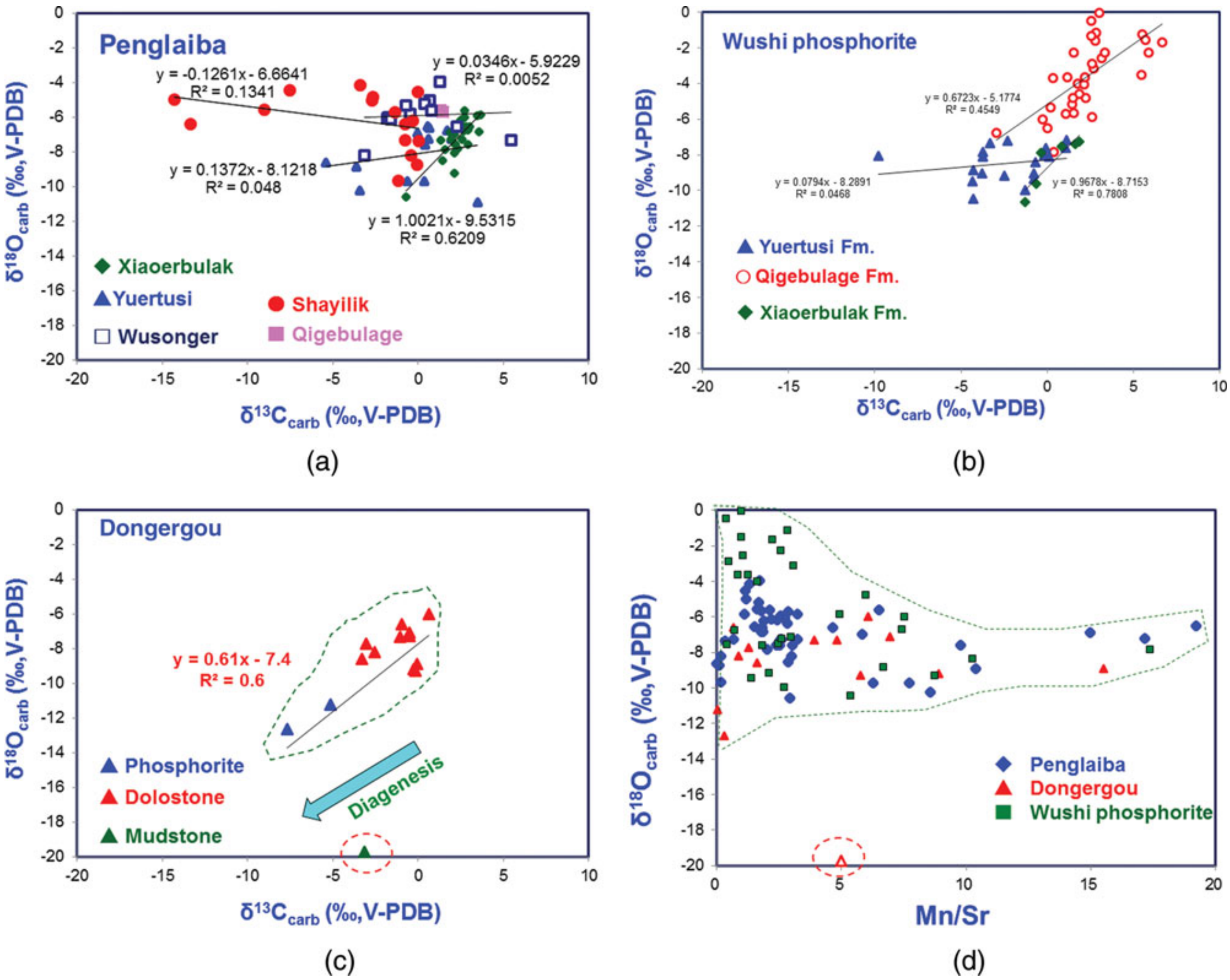

Figure 4. (Colour online) Cross-plot of $\delta^{18}O_{carb}$ and $\delta^{13}C_{carb}$ for the (a) Penglaiba, (b) Wushi phosphrite and (c) Dongergou sections and (d) $\delta^{18}O_{carb}$ and Mn/Sr (weight ratio).

The Xiaoerbulak Formation of the Penglaiba section and the Wushi phosphorite section consist of dolostone. Dolomitization is believed to affect the carbonate $\delta^{18}O$ value (Vasconcelos *et al.* 2005). Lower $\delta^{18}O$ values, reflecting a greater degree of alteration, becomes less useful in the case of dolomitization which can lead to higher $\delta^{18}O$ due to equilibrium isotopic fractionation (Li *et al.* 2011, 2013). Fluid–rock interaction shows the reset of $\delta^{18}O$ values without any significant effect on the $\delta^{13}C$ values (cf. Jacobsen & Kaufman, 1999), indicating that the $\delta^{13}C_{carb}$ values in dolostone reflect its near-primary composition although the $\delta^{18}O$ values have been affected by fluid–rock interactions.

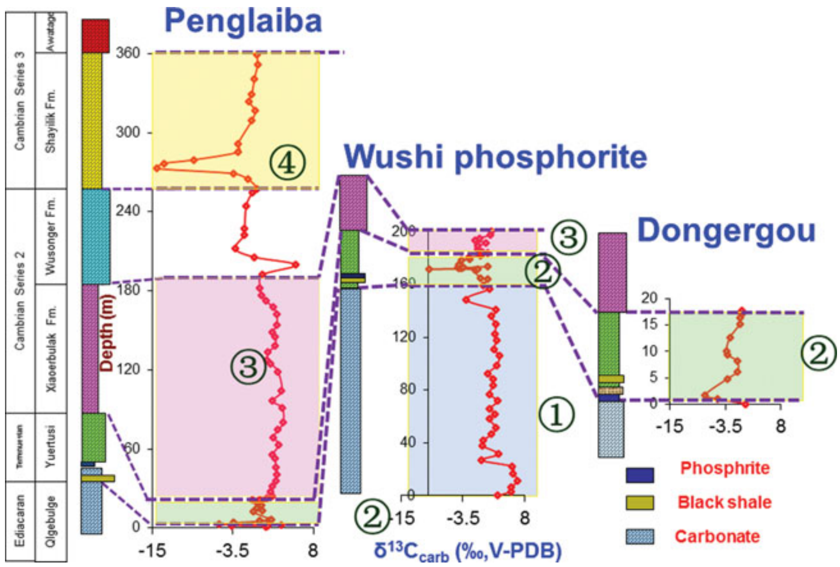

Figure 5. (Colour online) Stratigraphic variations of $\delta^{13}C_{carb}$ for the Penglaiba, Wushi phosphrite and Dongergou sections plotted against lithologic columns (①ED1; ②CAM1; ③CAM2; ④CAM3).

Mn/Sr and Mg/Ca ratios, as well as Mg, Fe, Mn, Sr and Ca abundances, are variable (Tables 1–3). No obvious correlation exists between Mn/Sr and the respective $\delta^{18}O$ values (Fig. 4d).

A few samples indicate that carbonates have been altered during diagenesis (e.g. DRG 9 shows a relatively low $\delta^{18}O$ value of –19.7 ‰, reflecting diagenetic alteration).

In summary, the absence of sufficient indication of post-depositional alteration in all three sections suggests that the carbonate carbon isotope records reflect near-primary values. This is discussed in the following section.

6. Discussion

6.a. Sections in the study

6.a.1. The Penglaiba section: variation in $\delta^{13}C_{carb}$

At Penglaiba, a sedimentary succession comprising the terminal Ediacaran and most of the Cambrian is exposed (Yu *et al.* 2004, 2009). The section represents a carbonate platform setting and provides the most complete carbonate carbon isotopic record of this study (Figs 3a, 5).

A shift in $\delta^{13}C_{carb}$ from 1.5 ‰ to a more negative value of –5.4 ‰ (②CAM1, Fig. 5) across the boundary between the Qigebulage Formation and the Yuertusi Formation is followed by rather invariable $\delta^{13}C_{carb}$ values between –0.6 ‰ and 2 ‰ in the middle and upper Yuertusi Formation. These in turn are followed by somewhat more variable and generally positive $\delta^{13}C_{carb}$ values between 1.3 ‰ and 3.7 ‰ in the Xiaoerbulak Formation, as well as more fluctuating $\delta^{13}C_{carb}$ values including a maximum value of about 5.4 ‰ in dolostones of the Wusonger Formation (③CAM2, Fig. 5).

The strongly negative $\delta^{13}C_{carb}$ excursion to values at –14.3 ‰ were observed near the base to the middle Shayilik Formation across the Cambrian Series 2 – Series 3 boundary (④CAM3, Fig. 5), followed by $\delta^{13}C_{carb}$ values around 0 ‰.

6.a.2. The Wushi phosphorite section

A positive $\delta^{13}C_{carb}$ excursion from 0 ‰ to 6.7 ‰ from the base to the upper Qigebulage Formation were observed (①ED1, Fig. 5), followed by a $\delta^{13}C_{carb}$ shift from 2.6 ‰ to –2.9 ‰ at the top of the Qigebulage Formation. The most negative $\delta^{13}C_{carb}$ value (–9.8 ‰) in the section occurs at the base of the Yuertusi Formation (②CAM1, Fig. 5). Moreover, a $\delta^{13}C_{carb}$ shift from –9.8 ‰ to 1.9 ‰ from the middle Yuertusi Formation to the base of the Xiaoerbulak Formation (③CAM2, Fig. 5) is apparent.

6.a.3. The Dongergou section

The carbonate carbon isotope record is based on 14 samples (Fig. 3c; Table 3). Similar to the results for the Penglaiba and the Wushi phosphorite sections, the most negative $\delta^{13}C_{carb}$ value of the Dongergou section with –7.7 ‰ is recorded at the base of the Yuertusi Formation (②CAM1, Fig. 5) followed by a $\delta^{13}C_{carb}$ shift towards –0.2 ‰ between the middle Yuertusi Formation and the base of the Xiaoerbulak Formation.

6.b. Comparison of the stratigraphy in the Tarim Basin

An overall increase in $\delta^{13}C_{carb}$ from 3 ‰ to 6.7 ‰ at the base of Qigebulage Formation is followed by a slight negative shift to nearly invariable values at the middle to the upper Qigebulage Formation (①ED1, Fig. 5) and a negative shift at the upper part of Qigebulage Formation. Further upsection, $\delta^{13}C_{carb}$

records a shift to minimum values of –9.8 ‰ in the Wushi phosphorite section to –7.7 ‰ in the Dongergou section and to –5.4 ‰ in the Penglaiba section. A shift to positive carbonate carbon isotope values occurs across the Yuertusi Formation in the middle of Xiaoerbulak Formation, followed by nearly invariable positive carbonate carbon isotope values between 1.4 ‰ and 3.7 ‰ for dolostones in the middle and upper Xiaoerbulak Formation (③CAM2, Fig. 5). Variable carbonate carbon isotope values are recorded for the Wusonger Formation. The most negative $\delta^{13}C_{carb}$ value occurs at the base of the Shayilik Formation (–14.3 ‰, Penglaiba section) (④CAM3, Fig. 5). The observation is probably as a result of the upwelling of water, with dissolved inorganic carbon carrying a ^{13}C depleted signature due to recycling of organic matter or enhanced weathering of organic-carbon-bearing rocks on the continents, and subsequent delivery of ^{13}C depleted dissolved inorganic carbon into the ocean; alternatively, it may be related to the enrichment of organic matter, which could be responsible for the observed change in $\delta^{13}C$ (Guo *et al.* 2010*a* , *b*). A positive carbonate carbon isotope excursion occurs in the middle–upper Shayilik Formation, indicating the recovery of the environment, increasing organic carbon burial and increasing carbon fixation.

6.c. Comparison between different continents

The Tarim Basin in NW China contains a sedimentary succession of Ediacaran and Cambrian rocks, including the deposition in different palaeoenvironmental settings (inner shelf, outer shelf, slope and basin). Three sections in the Keping area represent the carbonate platform environments. In the Tarim Basin, the Keping area exhibits a sedimentary succession and fossils comparable to the carbonate platform of the Yangtze Platform during the Ediacaran–Cambrian period (Chen *et al.* 2004, 2010; Sun *et al.* 2004; Feng *et al.* 2006; He, Xu & Yuan, 2007; Yu *et al.* 2009). The stratigraphic variation of the total carbon abundances shows a parallel evolution between the lower part of the Yuertusi Formation and the Niutitang Formation. All results from the study match previously published carbonate carbon isotope data from other sections on the Yangtze Platform (e.g. Zhang *et al.* 1997; Zhu *et al.* 2004; Zhu, Babcock & Peng, 2006; Guo *et al.* 2007, 2010*a*, *b*, 2013; G. Jiang *et al.* 2007, 2012; Yang *et al.* 2007; Zhu, Strauss & Shields, 2007; Li *et al.* 2013). The change in the carbon isotopic composition in the sequence of early Cambrian black rocks from the Yangtze Platform and the Tarim Basin is based on a large-scale transgressive event and interpreted as a change from anoxic to possibly dysoxic bottom-water conditions (S. Jiang *et al.* 2007; Guo *et al.* 2013).

Although defining the Ediacaran–Cambrian succession by $\delta^{13}C_{carb}$ data in these deeper water sections is problematic, respective $\delta^{13}C_{org}$ and $\delta^{13}C_{carb}$ data allow stratigraphic comparison of some sections of the Yangtze Platform (Zhang *et al.* 1997; Guo *et al.* 2007, 2013; S. Jiang *et al.* 2007; Yang *et al.* 2007; G. Jiang *et al.* 2012; Peng, Babcock & Cooper, 2012; Li *et al.* 2013) and also the Tarim Basin (Fig. 6).

A negative shift in $\delta^{13}C_{carb}$ (negative excursion at the base of the Cambrian System (BASE); Zhu, Babcock & Peng, 2006) from the base to the top of Qigebulage Formation and across the Ediacaran–Cambrian transition into the Yuertusi Formation can be observed. Moreover, more negative $\delta^{13}C_{carb}$ values can be observed at the base of the Yuertusi Formation in the Keping area, which can be compared with carbon isotope values from the transition of the Dengying Formation (Liuchapo Formation) and Niutitang Formation on the Yangtze Platform (Zhang *et al.* 1997; Zhu *et al.* 2004; Zhu, Babcock & Peng, 2006; Zhu, Strauss & Shields, 2007; Guo *et al.* 2007, 2013; G. Jiang *et al.* 2007, 2012; Yang *et al.* 2007; Li *et al.* 2013; Fig. 6). The $\delta^{13}C$ minimum reflects a global decrease in organic carbon burial and/or a decrease in carbon fixation, probably caused by a transgressive event (e.g. S. Jiang *et al.* 2007; Guo *et al.* 2013), flooding the shelf area with ^{13}C depleted basinal anoxic bottom water. The Ediacaran–Cambrian boundary in India (Kaufman *et al.* 2006), Iran (Brasier *et al.* 1990), Siberia (e.g. Magaritz *et al.* 1991; Brasier, Khomentovsky & Corfield, 1993; Brasier *et al.* 1994, 1998; Knoll *et al.* 1995*a* , *b*; Kouchinsky *et al.* 2007), Mongolia (Brasier *et al.* 1996; Khomentovsky & Gibsher, 1996; Maloof *et al.* 2010), Morocco (Maloof *et al.* 2005, 2010), Oman (Fike *et al.* 2006; Schröder & Grotzinger, 2007), the Yangtze Platform (e.g. Shen & Schidlowski, 2000; Zhu, Strauss & Shields, 2007; Guo *et al.* 2007, 2013; S. Jiang *et al.* 2007; G. Jiang *et al.* 2012; Peng, Babcock & Cooper, 2012; Li *et al.* 2013) and the Tarim Basin (this study) can be correlated with each other using the negative carbon isotope anomaly followed by a transition to less negative $\delta^{13}C$ values in lower Cambrian stratigraphy. A widespread transgressive event can be detected for lower Cambrian rocks on different continents (e.g. S. Jiang *et al.* 2007; Guo *et al.* 2013).

A distinct positive $\delta^{13}C_{carb}$ excursion from the Yuertusi Formation to the Xiaoerbulak Formation of the Penglaiba section reflects the enhanced fractional burial of organic matter and the release of oxygen. This excursion can be compared with the positive $\delta^{13}C_{carb}$ shift in the lower part of Cambrian Stage 2 (positive excursion in the lower part of Stage 2 (ZHUCE); Zhu, Babcock & Peng, 2006), which is the equivalent to the Dahai Member of the Xiaotan section in the shelf area of NE Yunnan, at 62 m of the Longbizui section and at 33 m at the Yuanjia section of the slope to basin area in the Yangtze Platform (Fig. 6; Zhu, Babcock & Peng, 2006; Li *et al.* 2013; Guo *et al.* 2013). Such a stratigraphic correlation is strongly supported by similar phosphorus-rich sediments between the ZHUCE-equivalent interval of the Penglaiba section, the Longbizui/Yuanjia sections and the Xiaotan section (Figs 2, 6).

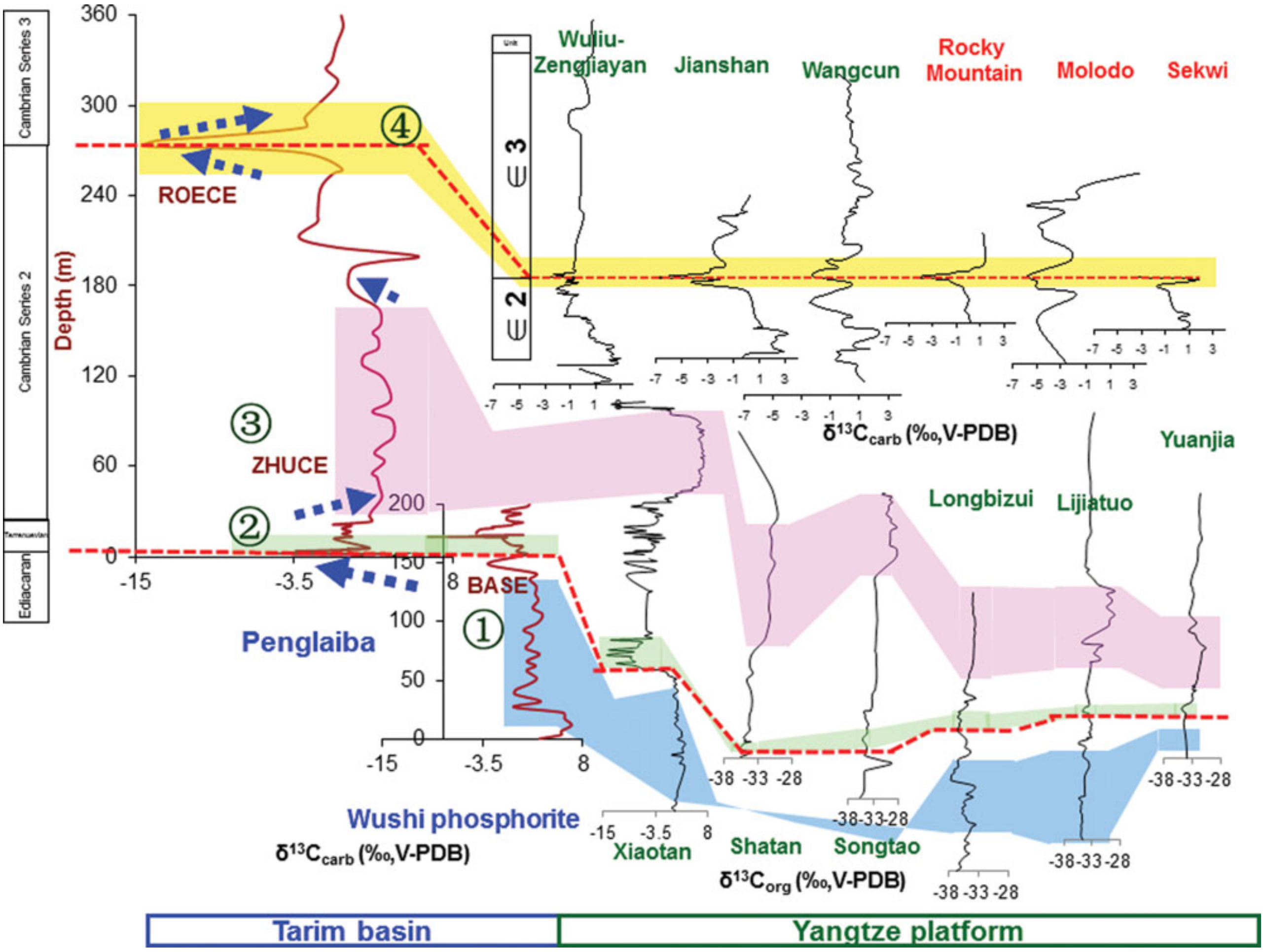

Figure 6. (Colour online) Comparison of temporal variations in $\delta^{13}C_{carb}$ from the different sections during the transition from the Ediacaran and Cambrian of (1) the Yangtze Platform, China: Shatan (Guo *et al.* 2007), Songtao (Guo *et al.* 2007), Yanwutan-Lijiatuo (Guo *et al.* 2007), Longbizui (Guo *et al.* 2013), Yuanjia (Guo *et al.* 2013), Xiaotan (Li *et al.* 2013), Wuliu–Zengjiayan (Guo *et al.* 2010), Jianshan (Guo *et al.* 2010*a* , *b*) and Wangcun sections (Zhu *et al.* 2004); (2) the Tarim Basin, China: Penglaiba (this study), Wushi phosphrite (this study) and Dongergou sections (this study); (3) USA: Rocky Mountain section (Montañez *et al.* 2000); (4) Russia: Molodo section (Shabanov *et al.* 2008); and (5) Canada: Sekwi Formation (Dilliard *et al.* 2007).

A linear evolution towards more ^{13}C-depleted carbonate carbon isotope values can be observed across the boundary of the Wusonger Formation and the Shayilik Formation at the Penglaiba section, with the most negative $\delta^{13}C_{carb}$ value of –14.3 ‰. This can be compared with the evolution of the carbonate carbon isotopes on the Yangtze Platform. The Cambrian Series 2 – Series 3 transition is characterized worldwide by a negative carbon isotope excursion caused by a transgressive event and biological radiation (*Redlichiid–Olenellid* extinction carbon isotope excursion or ROECE; Zhu, Babcock & Peng, 2006). The samples from the Penglaiba section show the most ^{13}C-depleted signature among Cambrian Series 2 and Cambrian Series 3, which could reflect a closer proximity to the source of ^{13}C-depleted water during upwelling (Guo *et al.* 2010*a* , *b*). Above the deposits of the transgressive event, the $\delta^{13}C_{carb}$ values increase again to values of *c.* 0 ‰, indicating the recovery in the marine environment, which is in accordance with values recorded for the Wuliu–Zengjiayan section and the Wangcun section on the Yangtze Platform (Zhu *et al.* 2004; Guo *et al.* 2010*a* , *b*). More evidence (Guo *et al.* 2010*a* , *b*) for this development is provided by the fact that the position of the observed negative shift in δ^{13}C can be correlated with a similar chemostratigraphic evolution in the sections of the Tarim Basin (this study) by a composite profile across the boundary from the Yangtze Platform (Zhu *et al.* 2004; Guo *et al.* 2010*a* , *b*), Canada (Dilliard *et al.* 2007), the USA (Montañez *et al.* 2000) and in respective successions in Siberia (Shabanov *et al.* 2008) (Fig. 6). The development of inhospitable bottom-water conditions due to the introduction of anoxic waters would undoubtedly result in faunal extinction (Guo *et al.* 2010*a* , *b*). The negative carbon isotope excursion and the trilobite mass extinction (e.g. Montañez *et al.* 2000) at the ROECE event in the uppermost part of Cambrian Series 2 and the lowermost part of Cambrian Series 3 were caused by major palaeogeographical changes coupled to the transgressive event (Guo *et al.* 2010*a* , *b*), which resulted in the deposition of transgressive successions visible in the Gondwana and Laurentia sections (e.g. Landing & Bartowski, 1996; Brasier & Sukhov, 1998; Montañez et al. 2000; Zhu et al. 2004; Wotte et al. 2007; Guo et al. 2010a , b; Figs 2, 6).

The carbon isotopic evolution recorded for the sections in the Tarim Basin is in good agreement with existing $\delta^{13}C$ records obtained from other sections on the Yangtze Platform that define the ZHUCE and the ROECE events (Zhu et al. 2004; Zhu, Babcock & Peng, 2006; Zhu, Strauss & Shields, 2007).

7. Conclusion

Complete high-resolution carbonate carbon isotope profiles across the Ediacaran–Cambrian and Cambrian Series 2 – Series 3 transitions in the Keping area of the Tarim Basin in NW China display clear stratigraphic variations. These can be correlated with the carbonate carbon isotope records for sedimentary successions on the Yangtze Platform. Isotope excursions reflect changes in the fractional burial of organic carbon, biological evolution and geological events. $\delta^{13}C_{carb}$ variations in the successions of the Tarim Basin and the Yangtze Platform correlate with each other and define the BASE, ZHUCE and the ROECE events. However, the global signature has been enhanced by a regional signal, likely as a consequence of differences in the palaeogeographical setting. These results reflect the perturbation of the carbon cycle in the Tarim Basin during the Ediacaran–Cambrian and the Cambrian Series 2 – Series 3 transitions.

Acknowledgements. The authors appreciate the assistance and expertise in the field as well as stimulating discussions with Professor Harald Strauss, Dr Marc Peters, Professor Bingsong Yu, Professor Xianhua Li, Professor Maoyan Zhu, Dr Chukwunonso Peter Okoli and Mr Yue Chen. GQ acknowledges financial support from 973 Program (no. 2013CB835004) and the National Natural Science Foundation of China (NSFC nos 41473018, 41625006 and 41173008).

References

Brasier, M. D., Khomentovsky, V. V. & Corfield, R. M. 1993. Stable isotopic calibration of the earliest skeletal fossil assemblages in eastern Siberia (Precambrian-Cambrian boundary). *Terra Nova* **5**, 225–32, doi: 10.1111/j.1365-3121.1993.tb00253.x.

Brasier, M. D., Magaritz, M., Corfeld, R., et al. 1990. The carbon-and oxygen-isotopic record of the Precambrian–Cambrian boundary interval in China and Iran and their correlation. *Geological Magazine* **127**, 319–32.

Brasier, M. D., Rozanov, A. Yu., Zhuravlev, A. Yu., Corfield, R. M. & Derry, L. A. 1994. A carbon isotope reference scale for the Lower Cambrian succession in Siberia: report of IGCP Project 303. *Geological Magazine* **131**, 767–83.

Brasier, M. D., Shields, G., Kuleshov, V. N. & Zhegallo, E. A. 1996. Integrated chemo- and biostratigraphic calibration of early animal evolution: Neoproterozoic–Early Cambrian of southwest Mongolia. *Geological Magazine* **133**, 445–85, doi: 10.1017/S0016756800007603.

Brasier, M. D. & Sukhov, S. S. 1998. The falling amplitude of carbon isotopic oscillations through the Lower to Middle Cambrian: northern Siberia data. *Canadian Journal of Earth Sciences* **35**, 353–73.

Chen, J., Sun, S., Liu, W. & Zheng, J. 2004. Geochemical characteristics and genesis of organic rich layers of Lower Cambrian from northern Tarim Basin. *Science China (D)* **34**(S-I), 107–13.

Chen, Y., Jiang, S., Zhou, X., Yang, W. & Han, L. 2010. $\delta^{30}Si$, $\delta^{18}O$ and elements geochemistry on the bedded siliceous rocks and cherts in dolostones from Cambrian strata, Tarim Basin. *Geochimica* **39**(2), 159–70.

Dilliard, K. A., Pope, M. C., Coniglio, M., Hasiotis, S. T. & Lieberman, B. S. 2007. Stable isotope geochemistry of the lower Cambrian Sekwi Formation, Northwest Territories, Canada: Implications for ocean chemistry and secular curve generation. *Palaeogeography, Palaeoclimatology, Palaeoecology* **256**, 174–94.

Feng, L., Li, C., Huang, J., Chang, H. & Chu, X. 2014. A sulfate control on marine mid-depth euxinia on the early Cambrian (ca. 529-521 Ma) Yangtze Platform, South China. *Precambrian Research* **246**, 123–33.

Feng, Z., Bao, Z., Wu, M., et al. 2006. Lithofacies palaeogeography of the Cambrian in Tarim area. *Journal of Palaeogeography* **8**(4), 427–39.

Fike, D. A., Grotzinger, J. P., Pratt, L. M. & Summons, R. E. 2006. Oxidation of the Ediacaran Ocean. *Nature* **444**, 744–7.

Guo, Q., Strauss, H., Liu, C., Goldberg, T., Zhu, M., Heubeck, C., Pi, D., Vernhet, E., Yang, X. & Fu, P. 2007. Carbon isotopic evolution of the terminal Neoproterozoic and Early Cambrian: evidence from the Yangtze Platform, South China. *Palaeogeography, Palaeoclimatology, Palaeoecology* **254**, 140–57.

Guo, Q., Strauss, H., Liu, C., Zhao, Y., Yang, X., Peng, J. & Yang, H. 2010a. A negative carbon isotope excursion defines the transition from Cambrian Series 2 to Cambrian Series 3 on the Yangtze Platform, South China. *Palaeogeography, Palaeoclimatology, Palaeoecology* **285**, 143–51.

Guo, Q., Strauss, H., Liu, C., Zhao, Y., Yang, X., Peng, J. & Yang, H. 2010b. Corrigendum to "A negative carbon isotope excursion defines the boundary from Cambrian Series 2 to Cambrian Series 3 on the Yangtze Platform, South China". *Palaeogeography, Palaeoclimatology, Palaeoecology* **285**, 143–51.

Guo, Q., Strauss, H., Zhao, Y., Yang, X., Peng, J., Yang, Y. & Deng, Y. 2014. Reconstructing marine redox conditions for the transition between Cambrian Series 2 and Cambrian Series 3, Kaili area, Yangtze Platform: Evidence from biogenic sulfur and degree of pyritization. *Palaeogeography, Palaeoclimatology, Palaeoecology* **398**, 144–53.

Guo, Q., Strauss, H., Zhu, M., Zhang, J., Yang, X., Lu, M. & Zhao, F. 2013. High-resolution organic carbon isotope stratigraphy from a slope to basinal setting on the Yangtze Platform, South China: Implications for the Ediacaran-Cambrian transition. *Precambrian Research* **225**, 209–17.

He, X., Xu, B. & Yuan, Z. 2007. The carbon isotope composition and comparison of late Neoproterozoic strata in the Xinjiang Keping area. *Chinese Science Bulletin* **52**(1), 107–13.

Jacobsen, S. B. & Kaufman, A. J. 1999. The Sr, C and O isotopic evolution of Neoproterozoic seawater. *Chemical Geology* **161**, 37–57.

Jiang, G., Kaufman, A. J., Christie-Blick, N., Zhang, S. & Wu, H. 2007. Carbon isotope variability across the

Ediacaran Yangtze platform in South China: implications for a large surface-to-deep ocean $\delta^{13}C$ gradient. *Earth and Planetary Science* **261**, 303–20.

Jiang, G., Wang, X., Shi, X., *et al.* 2012. The origin of decoupled carbonate and organic carbon isotope signatures in the early Cambrian (ca. 542–520 Ma) Yangtze platform. *Earth and Planetary Science Letters* **317–8**, 96–110.

Jiang, S., Yang, J., Ling, H., Chen, Y., Feng, H., Zhao, K. & Ni, P. 2007. Extreme enrichment of polymetallic Ni–Mo–PGE–Au in lower Cambrian black shales of South China: an Os isotope and PGE geochemical investigation. *Palaeogeography, Palaeoclimatology, Palaeoecology* **254**, 217–28.

Kaufman, A. J., Jacobsen, S. B. & Knoll, A. H. 1993. The Vendian record of Sr- and C-isotopic variations in seawater: implications for tectonic and paleoclimate. *Earth and Planetary Science Letters* **120**, 409–30.

Kaufman, A. J., Jiang, G., Christie-Blick, N., Banerjee, D. M. & Rai, V. 2006. Stable isotope record of the terminal Neoproterozoic Krol platform in the Lesser Himalayas of northern India. *Precambrian Research* **147**, 156–85.

Kaufman, A. J. & Knoll, A. H. 1995. Neoproterozoic variations in the C-isotopic composition of seawater: stratigraphic and biogeochemical implications. *Precambrian Research* **73**, 27–49.

Khomentovsky, V. V. & Gibsher, A. S. 1996. The Neoproterozoic–Lower Cambrian in northern Govi-Altay, western Mongolia: regional setting, lithostratigraphy and biostratigraphy. *Geological Magazine* **133**, 371–90, doi: 10.1017/S001675680000755X.

Knoll, A. H. 1991. End of the Proterozoic Eon. *Scientific American* **265**, 64–73.

Knoll, A. H., Grotzinger, J. P., Kaufman, A. J. & Kolosov, P. 1995a. Integrated approaches to terminal Proterozoic stratigraphy: an example from the Olenek Uplift, northeastern Siberia. *Precambrian Research* **73**, 251–70, doi: 10.1016/0301-9268(94)00081-2.

Knoll, A. H., Kaufman, A. J., Semikhatov, M. A., Grotzinger, J. P. & Adams, W. 1995b. Sizing up the sub-Tommotian unconformity in Siberia. *Geology* **23**, 1139–43, doi: 10.1130/0091-7613(1995)023 <1139: SUTSTU>2.3.CO;2.

Kouchinsky, A., Bengtson, S., Pavlov, V., Runnegar, B., Torssander, P., Young, E. & Ziegler, K. 2007. Carbon isotope stratigraphy of the Precambrian-Cambrian Sukharikha River section, northwestern Siberian platform. *Geological Magazine* **144**, 609–18, doi: 10.1017/S0016756807003354.

Landing, E. & Bartowski, K. E. 1996. Oldest shelly fossils fromthe Taconic allochthon and late Early Cambrian sea-levels in eastern Laurentia. *Journal of Paleontology* **70**, 741–61.

Li, C., Love, G. D., Lyons, T. W., Fike, D. A., Sessions, A. L. & Chu, X. 2010. A Stratified Redox Model for the Ediacaran Ocean. *Science* **328**(5974), 80–3.

Li, D., Ling, H., Shields-Zhou, G. A., Chen, X., Cremonese, L., Och, L., Thirlwall, M., Christina, J. & Mannin, C. J. 2013. Carbon and strontium isotope evolution of seawater across the Ediacaran–Cambrian transition: Evidence from the Xiaotan section, NE Yunnan, South China. *Precambrian Research* **225**, 128–47.

Li, D., Shields-Zhou, G., Ling, H.-F. & Thirlwall, M. 2011. Dissolution methods for strontium isotope stratigraphy: guidelines for the use of bulk marine carbonate and phosphorite rocks. *Chemical Geology* **290**, 133–44.

Li, R., Chen, J., Zhang, S., Lei, J., Shen, Y. & Chu, X. 1999. Spatial and temporal variations in carbon and sulfur isotopic compositions of Sinian sedimentary rocks in the Yangtze platform, South China. *Precambrian Research* **97**, 59–75.

Magaritz, M., Kirschvink, J. L., Latham, A. J., Zhuravlev, A. Yu. & Rozanov, A. Yu. 1991. Precambrian/Cambrian boundary problem: carbon isotope correlations for Vendian and Tommotian time between Siberia and Morocco. *Geology* **19**, 847–50, doi: 10.1130/ 0091-7613(1991) 019<0847: PCBPCI>2.3.CO;2.

Maloof, A. C., Schrag, D. P., Crowley, J. L. & Bowring, S. A. 2005. An expanded record of Early Cambrian carbon cycling from the Anti-Atlas margin, Morocco. *Canadian Journal of Earth Sciences* **42**, 2195–216, doi: 10.1139/e05-062.

Maloof, A. C., Susannah, M. P., Moore, J. L., Dudás, F. Ö., Samuel, A. B., Higgins, J. A., Fike, D. A. & Eddy, M. P. 2010. The earliest Cambrian record of animals and ocean geochemical change. *Geological Society of America Bulletin* **122**, 1731–74.

Marshall, J. D. 1992. Climatic and oceanographic isotopic signals from the carbonate rock record and their preservation. *Geological Magazine* **129**, 143–60.

McCrea, J. M. 1950. On the isotopic chemistry of carbonates and a paleotemperature scale. *Journal of Chemical Physics* **18**, 849–57.

McKerrow, W. S., Scotese, C. R. & Brasier, M. D. 1992. Early Cambrian continental reconstructions. *Journal of the Geological Society,* London **149**, 599–606.

Montañez, I. P., Osleger, D. A., Banner, J. L., Mack, L. E. & Masgrove, M. L. 2000. Evolution of the Sr and C isotope composition of Cambrian oceans. *GSA Today* **10**, 1–7.

Och, L. M., Cremonese, L., Shields-Zhou, G. A., Poulton, S. W., Struck, U., Ling, H., Li, D., Chen, X., Manning, C., Thirlwall, M., Strauss, H. & Zhu, M. 2016. Palaeoceanographic controls on spatial redox distribution over the Yangtze Platform during the Ediacaran-Cambrian transition. *Sedimentology* **63**(2), 378–410.

Peng, S. 2009. The newly developed Cambrian biostratigraphic succession and chronstratigraphic scheme for South China. *Chinese Science Bulletin (English Edition)* **54**, 4161–79.

Peng, S., Babcock, L. E. & Cooper, R. A. 2012. The Cambrian Period. In *The Geological Time Scale*, Volume 2 (eds F. M. Gradstein, J. G. Ogg, M. D. Schmitz & G. M. Ogg), pp. 437–88. Amsterdam: Elsevier BV, 1144 pp.

Popp, B. N., Anderson, T. F. & Sandberg, P. A. 1986. Textural, elemental and isotopic variations among constituents in Middle Devonian limestones, North America. *Journal of Sedimentary Petrology* **56**, 715–27.

Saltzman, M. R., Ripperdan, R. L., Brasier, M. D., Lohmann, K. C., Robison, R. C., Chang, W. T., Peng, S., Ergaliev, E. K. & Runnegar, B. R. 2000. A global carbon isotope excursion (SPICE) during the Late Cambrian: relation to trilobite extinction, organic-matter burial, and sea level. *Palaeogeography, Palaeoclimatology, Palaeoecology* **160**, 211–23.

Saltzman, M. R., Runkel, A. C., Cowan, C. A., Runnegar, B., Stewart, M. C. & Palmer, A. R. 2004. The upper Cambrian SPICE ($\delta^{13}C$) event and the Sauk II–Sauk III regression: new evidence from Laurentian basins in Utah, Iowa and Newfoundland. *Journal of Sedimentary Research* **74**, 366–77.

SALTZMAN, M. R., RUNNEGAR, B. & LOHMANN, K. C. 1998. Carbon isotope stratigraphy of Upper Cambrian (Steptoean Stage) sequences of the eastern Great Basin: Record of a global oceanographic event. *Geological Society of America Bulletin* **110**, 285–97.

SAWAKI, Y., OHNO, T., FUKUSHI, Y., *et al*. 2008. Sr isotope excursion across the Precambrian-Cambrian boundary in the Three Gorges area, South China. *Gondwana Research* **14**, 134–47.

SCHRAG, D. P., HIGGINS, J. A., MACDONALD, F. A. & JOHNSTON, D. T. 2013. Authigenic carbonate and the history of the Global Carbon Cycle. *Science* **339**, 540–43.

SCHRÖDER, S. & GROTZINGER, J. P. 2007. Evidence for anoxia at the Ediacaran-Cambrian boundary: the record of redox-sensitive trace elements and rare earth elements in Oman. *Journal of the Geological Society* **164**, 175–87.

SCOTESE, C. R. & MCKERROW, W. S. 1990. Revised world maps and introduction. In *Palaeozoic Palaeogeography and Biogeography* (eds W. S. McKerrow & C. R. Scotese), pp. 1–21. Geological Society of London, Memoir no. 12.

SHABANOV, YU. YA., KOROVNIKOV, I. V., PERELADOV, V. S., PAK, K. L. & FEFLOV, A. F. 2008. Proposed global standard stratotype-section and point for the Amganian Stage (Cambrian): Kuonamka Formation section along the Molodo River, western Yakutia, Russia. *The 13th International Field Conference of the Cambrian Stage Subdivision Working Group (Siberian Platform, Western Yakutia)*, 60–70.

SHEN, Y. & SCHIDLOWSKI, M. 2000. New C isotope stratigraphy from southwest China: implications for the placement of the Precambrian–Cambrian boundary on the Yangtze Platform and global correlations. *Geology* **28**, 623–6.

SHIELDS-ZHOU, G. A. & OCH, L. 2011. The case for a Neoproterozoic Oxygenation Event: Geochemical evidence and biological consequences. *GSA Today* **21**, 4–11.

SUN, X., CHEN, J., ZHENG, J. & LIU, W. 2004. Geochemical characteristics of organic matter rich sedimentary strata in Lower Cambrian, Tarim Basin and its origins. *Acta Sedimentologica Sinica* **22**(3), 547–52.

VASCONCELOS, C., MCKENZIE, J. A., WARTHMANN, R. & BERNASCONI, S. M. 2005. Calibration of the delta O-18 paleothermometer for dolomite precipitated in microbial cultures and natural environments. *Geology* **33**, 317–20.

VEIZER, J. 1983. Chemical diagenesis of carbonates: theory application. In: *Stable Isotopes in Sedimentary Geology* (eds M. A. Arthur *et al*.). SEPM, Tulsa, Society of Economic Palaeontologists and Mineralogists, Short Course, 10.

VEIZER, J., ALA, D., AZMY, K., BRUCKSCHEN, P., BUHL, D., BRUHN, F., CARDEN, G. A. F., DIENER, A., EBNETH, S., GODDERIS, Y., JASPER, T., KORTE, C., PAWELLEK, F., PODLAHA, O. G. & STRAUSS, H. 1999. $^{87}Sr/^{86}Sr$, $\delta^{13}C$ and $\delta^{18}O$ evolution of Phanerozoic seawater. *Chemical Geology* **161**, 59–88.

VEIZER, J., BRUCKSCHEN, P., PAWELLEK, F., DIENER, A., PODLAHA, O. G., CARDEN, G. A. F., JASPER, T., KORTE, C., STRAUSS, H., AZMY, K. & ALA, D. 1997. Oxygen isotope evolution of Phanerozoic seawater. *Palaeogeography, Palaeoclimatology, Palaeoecology* **132**, 159–72.

WACHTER, E. A. & HAYES, J. M. 1985. Exchange of oxygen isotopes and carbon isotopes in carbon dioxide-phosphoric acid systems. *Chemical Geology* **52**, 365–74.

WANG, D., STRUCK, U., LING, H., GUO, Q., SHIELDS-ZHOU, G. A., ZHU, M. & YAO, S. 2015. Nitrogen isotope study of black shales during Early Cambrian on Yangtze platform, South China. *Precambrian Research* **267**, 209–26.

WOTTE, T., ÁLVARO, J. J., SHIELDS, G. A., BROWN, B., BRASIER, M. D. & VEIZER, J. 2007. C-, O- and Srisotope stratigraphy across the Lower–Middle Cambrian transition of the Cantabrian Zone (Spain) and the Montagne Noire (France), West Gondwana. *Palaeogeography, Palaeoclimatology, Palaeoecology* **256**, 47–70.

YANG, X., ZHU, M., GUO, Q. & ZHAO, Y. 2007. Organic carbon isotopic evolution during the Ediacaran-Cambrian transition interval in Eastern Guizhou, South China: paleoenvironmental and stratigraphic implications. *Acta Geologica Sinica (English Edition)* **81**(2), 194–203.

YU, B., CHEN, J., LI, X. & LIN, C. 2004. Rare earth and trace element patterns in bedded cherts from the bottom of the Lower Cambrian in the northern Tarim Basin, northwest China: implication for depositional environments. *Acta Sedimentologica Sinica* **22**(1), 59–66 (in Chinese with English abstract).

YU, B., DONG, H., WIDOM, E., CHEN, J. & LIN, C. 2009. Geochemistry of basal Cambrian black shales and cherts from the Northern Tarim Basin, Northwest China: Implications for depositional setting and tectonic history. *Journal of Asian Earth Sciences* **34**, 418–36.

ZHANG, J., LI, G., ZHOU, C., ZHU, M. & YU, Z. 1997. Carbon isotope profiles and their correlation across the Neoproterozoic Cambrian boundary interval on the Yangtze Platform, China. *Bulletin of National Museum of Natural Science* **10**, 107–16.

ZHAO, Y. & ZHENG, Y. 2010. Stable isotope evidence for involvement of deglacial meltwater in Ediacaran carbonates in South China. *Chemical Geology* **271**, 86–100.

ZHOU, C. & XIAO, S. 2007. Ediacaran $\delta^{13}C$ chemostratigraphy of South China. *Chemical Geology* **237**, 107–26.

ZHOU, Z. 2001. *Stratigraphy of the Tarim Basin*. Beijing: Science Press (in Chinese).

ZHU, M., BABCOCK, L. E. & PENG, S. C. 2006. Advances in Cambrian Stratigraphy and paleontology: Integrating correlation techniques, palaeobiology, taphonomy and paleoenvironmental reconstruction. *Palaeoworld* **15**, 217–22.

ZHU, M., STRAUSS, H. & SHIELDS, G. A. 2007. From snowball earth to the Cambrian bioradiation: Calibration of Ediacaran-Cambrian earth history in South China. *Palaeogeography, Palaeoclimatology, Palaeoecology* **254**, 1–6.

ZHU, M., ZHANG, J., LI, G. & YANG, A. 2004. Evolution of C isotopes in the Cambrian of China: implications for Cambrian subdivision and trilobite mass extinctions. *Geobios* **37**, 287–301.

ZHU, M., ZHANG, J., STEINER, M. & YANG, A. 2003. Sinian-Cambrian stratigraphic framework for shallow- to deep-water environments of the Yangtze Platform: an integrated approach. *Progress in Natural Science* **13**(12), 951–60.